A Novel Robotic Platform for Laser-Assisted Transurethral Surgery of the Prostate

S. Russo*, *Student Member, IEEE*, P. Dario, *Fellow, IEEE*, and A. Menciassi, *Member, IEEE*

***Abstract*—Benign prostatic hyperplasia (BPH) is the most common pathology afflicting ageing men. The gold standard for the surgical treatment of BPH is transurethral resection of the prostate. The laser-assisted transurethral surgical treatment of BPH is recently emerging as a valid clinical alternative. Despite this, there are still some issues that hinder the outcome of laser surgery, e.g., distal dexterity is strongly reduced by the current endoscopic instrumentation and contact between laser and prostatic tissue cannot be monitored and optimized. This paper presents a novel robotic platform for laser-assisted transurethral surgery of BPH. The system, designed to be compatible with the traditional endoscopic instrumentation, is composed of a catheter-like robot provided with a fiber optic-based sensing system and a cable-driven actuation mechanism. The sensing system allows contact monitoring between the laser and the hypertrophic tissue. The actuation mechanism allows steering of the laser fiber inside the prostatic urethra of the patient, when contact must be reached. The design of the proposed robotic platform along with its preliminary testing and evaluation is presented in this paper. The actuation mechanism is tested in *in vitro* experiments to prove laser steering performances according to the clinical requirements. The sensing system is calibrated in experiments aimed to evaluate the capability of discriminating the contact forces, between the laser tip and the prostatic tissue, from the pulling forces exerted on the cables, during laser steering. These results have been validated demonstrating the robot's capability of detecting sub-Newton contact forces even in combination with actuation.**

***Index Terms*—Benign prostatic hyperplasia (BPH), Bragg gratings, laser-assisted surgery, steerable surgical tool, surgical robotics.**

I. Introduction

ROBOTIC technology has gained a wide acceptance in the field of urology in the last decades [1], since the first robotic platform was proposed for prostate resection [2]. In 2011, the 83% of prostatectomy operations in USA were performed with the da Vinci Surgical System, Intuitive Surgical, Sunnyvale, CA, USA. Nevertheless, prostatectomy performed with the da Vinci Surgical System in 2012 were 15% below 2011 (http://www.intuitivesurgical.com/), but this could depend on improved prevention and change in treatment recommendations for the low-risk prostate cancer away from the definitive treatment.

In addition, many research robotic platforms have been studied and developed in the last years for urologic applications. A robotic system for transurethral inspection of bladder urothelium and tumor resection is presented in [3]. An active remote steering mechanism for bladder cancer detection and postoperative surveillance is proposed in [4]. The Hansen Medical Inc. robotic platform was adapted and tested for visual inspection of the interior of the urethra and kidneys in [5]. The feasibility and safety of an MR imaging-controlled transurethral ultrasound therapy robotic system for prostate cancer is evaluated in [6]. Robotic systems for precise needle insertion in the prostate under continuous magnetic resonance imaging (MRI) guidance are discussed in [7] and [8]. Hashimoto *et al.* in [9] proposed a manipulator for transurethral resection of the prostate, provided with a prostate displacement mechanism and a continuous perfusion resection system. Pantuck *et al.* presented in [10] a tool to improve the efficacy and safety during transurethral endoscopic surgery. A robotic system to perform transurethral ultrasound scanning, surgical motion planning, execution, and virtual evaluation of transurethral laser resection is introduced in [11].

Recently, the application of lasers in urology has undergone significant advances [12]. In particular, laser-assisted procedures are emerging as a valid clinical alternative to transurethral resection of the prostate (TURP) for the treatment of benign prostatic hyperplasia (BPH). Despite this, there are still some issues that hamper the widespread of this technology, e.g., distal dexterity is highly reduced and contact between laser and prostatic tissue cannot be controlled. These limitations may influence the outcome of surgery since, with some laser types, the prostatic tissue can be ablated only when in direct contact with the laser [13], [14]. Refinements to existing technology could increase the role of lasers in BPH surgical treatment; in particular, a significant advance could be introduced by the merging of robotics with minimally invasive laser techniques. Among the robotic platforms described previously, laser technology is integrated only in [3] and [11], respectively, for bladder and prostate tumors. No robotic platforms exist for laser-assisted BPH surgery combining distal dexterity and direct contact monitoring at the surgical tool.

In this paper, the design of the ASTRO (actuated and sensorised tool for laser-assisted surgery of the prostate), a novel robotic platform for transurethral laser surgery of BPH, is presented along with its preliminary evaluation. This system combines at the same time contact monitoring at the surgical site and distal dexterity, while maintaining a small distal overall

Manuscript received April 16, 2014; revised July 4, 2014 and August 9, 2014; accepted September 9, 2014. Date of publication September 17, 2014; date of current version January 16, 2014. This work was supported by the MILoRDS Project (Minimally Invasive Laser Robotic assisted Diagnosis and Surgery) funded by Tuscany Region, POR CReO Fesr 2007-2013. *Asterisk indicates corresponding author.*

*S. Russo is with the The BioRobotics Institute, Scuola Superiore Sant'Anna, 56025 Pontedera, Italy (e-mail: s.russo@sssup.it).

P. Dario and A. Menciassi are with The BioRobotics Institute, Scuola Superiore Sant'Anna, 56025 Pontedera, Italy (e-mail: p.dario@sssup.it; a.menciassi@sssup.it).

Color versions of one or more of the figures in this paper are available online at http://ieeexplore.ieee.org.

Digital Object Identifier 10.1109/TBME.2014.2358711

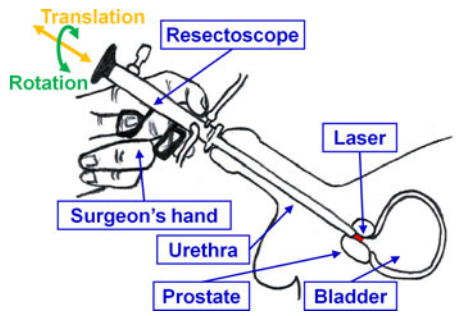

Fig. 1. Overview of the laser-assisted transurethral surgical procedure of BPH. The resectoscope is inserted through the urethra to access the prostate. The surgeon can move the resectoscope by translating and rotating it along/about its longitudinal axis.

encumbrance. The ASTRO is designed to be compatible with current commercial endoscopic instrumentation, thus avoiding the necessity for dedicated or customized instruments.

II. Clinical Motivations

BPH is a nonmalignant enlargement of the prostate that may compress or cause an occlusion of the urethra: It is the most common pathology afflicting ageing men and constitutes a major factor impacting male health [15]. BPH can lead to symptoms that affect quality of life and sleeping patterns, such as urgency to urinate, frequent urination, weak stream, straining, and/or the sensation of incomplete bladder emptying. In the most severe stage of BPH, the inability to completely empty the bladder may progress to complete urinary blockage, which can in turn lead to kidney damage [16].

The gold standard for the surgical treatment of BPH is TURP. TURP is performed through the resectoscope, an endoscopic straight instrument that is composed of three elements: a working element provided with an operative channel for the surgical tool insertion, optics for visualization of the surgical site and a sheath with irrigating fluid valves. In TURP, a wire-loop electrode for cutting and coagulating is inserted by the surgeon through the operative channel. The procedure requires general or spinal anesthesia. This operation has disadvantages such as blood loss requiring transfusion, incontinence, impotence, long postoperative catheterization time, etc. [16].

In recent years, other surgical techniques have been proposed in order to find a valid alternative to TURP (in 2005, only 39% of BPH surgeries were TURP according to [17]), providing the same clinical outcome while reducing the intra and postoperative complications. In particular, laser-assisted procedures allow reducing intraoperative blood loss as well as postoperative bleeding, catheterization time, invasiveness of the surgical procedure, duration of hospital stay, and recovery time [18].

The laser-assisted treatment of BPH is performed transurethrally via the resectoscope similarly as TURP, as shown in Fig. 1. In the last decades, various lasers have been introduced for the treatment of BPH [14], [19] including neodymium:yttrium–aluminum–garnet (Nd:YAG), potassium titanyl phosphate:yttrium–aluminum–garnet (KTP:YAG), diode laser, holmium:yttrium–aluminum–garnet (Ho:YAG), and thulium:yttrium–aluminum–garnet (Tm:YAG). Depending on laser wavelength, laser interaction with tissue can be different: laser radiation can be absorbed by water or hemoglobin in prostate tissue. The Nd:YAG laser produces energy at a wavelength of 1060 nm and it has an optical penetration depth (OPD) in prostatic tissue of 3 mm. The Nd:YAG laser radiation is transmitted in noncontact mode because the laser radiation is absorbed by the hemoglobin in the tissue. The KTP:YAG laser has a wavelength of 532 nm and an OPD in prostatic tissue of 0.8 mm. KTP:YAG laser energy is selectively absorbed within the tissue by hemoglobin (similarly as Nd:YAG laser), therefore, it does not require contact with target tissue. Diode lasers for the prostate treatment are available at various wavelengths 940, 980, or 1470 nm that are all absorbed by both water and hemoglobin. A diode laser can be pulsed or continuous and have different OPDs. The Ho:YAG laser is a pulsed laser with a wavelength of 2120 nm, the OPD in prostatic tissue is 0.4 mm. The laser energy of the Ho:YAG laser is highly absorbed by water (resulting in rapid dispersion of heat) and requires a contact with the target tissue; if used in noncontact mode, the efficiency of tissue vaporization is reduced. The Tm:YAG laser operates continuously at a wavelength of 2000 nm. Similarly to Ho:YAG, the Tm:YAG offers complete absorption of laser energy in water and it requires contact with target tissue. The OPD in prostatic tissue is 0.25 mm.

Different laser surgical techniques for the prostate treatment have been studied [14], [18], [19] based on the different wavelength dependent laser–prostatic tissue interactions: coagulation and vaporization. Vaporization is used in different ways to achieve different treatments that range from complete tissue vaporization to incision, resection, or enucleation. Visual laser ablation of the prostate (VLAP) and interstitial laser coagulation (ILC) are based on the principle of laser coagulation. During VLAP, Nd:YAG laser energy is delivered to the prostate gland with a side-firing, noncontact, free-beam laser. The ILC is performed with diode or Nd:YAG laser. The optical fiber is inserted directly into the prostate gland, and the laser energy is emitted into the tissue. The VLAP and ILC have mostly been abandoned because of long postoperative catheterization, unpredictable outcomes, and high reoperation rates [14]. In laser vaporization, laser energy is delivered with a contact or noncontact laser fiber causing the tissue to vaporize (at around 100 °C). Photoselective vaporization of the prostate (PVP) is mainly performed with KTP:YAG. With the recent commercial availability of higher power, 80-W KTP lasers, such as the "GreenLight" laser, higher tissue vaporization rates can be achieved. KTP laser vaporization has a relatively short learning curve and can be performed safely but no tissue for histological evaluation is obtained. Furthermore, KTP:YAG laser fiber are single use (and cost about 1000 Euro per patient) while Holmium laser fibers can be resterilized (cost per patients are about 20 Euro) [18]. Holmium laser ablation of the prostate (HoLAP) is based on the principle of vaporization. HoLAP procedures were initially performed using 60-W systems and side-firing laser fibers. It was considered to be a time-consuming procedure and limited to use in smaller prostates but, with the recent introduction of higher power Ho:YAG lasers (100–120 W), HoLAP is being

reexplored for small and medium-sized prostates because procedure times is reduced. HoLRP is based on the principle of laser vaporization. The energy is delivered to the prostate in contact mode through an end or side-firing fiber. This procedure does not completely vaporize the tissue, therefore, some tissue specimen for histological examination can be obtained (differently from HoLAP and PVP). The prostate is resected into chips small enough to be retrieved from the bladder through a standard resectoscope. Larger prostates take more time to resect, making them less suitable for this method. The Holmium laser enucleation of the prostate principle of operation is similar to HoLRP, in that it is based on the principle of tissue vaporization with a contact laser fiber. This procedure is mainly executed with end fire fibers. Here, the entire lobes are enucleated intact from the prostatic capsule, pushed up into the bladder, mechanically morcellated into smaller pieces, and then, flushed out of the urinary system. This technique is faster than HoLRP and can be used on larger prostate glands. The Tm:YAG laser is currently been studied for ablation, resection and enucleation of the prostate almost identically to Ho:YAG. Rapid absorption in water, short penetration depth and incisional and haemostatic properties are similar to those of the Ho:YAG, but the cutting is smoother owing to the continuous mode.

Laser-assisted BPH procedures are performed through the resectoscope (see Fig. 1) that is a telescopic straight and rigid instrument allowing only translation and rotation along/about its longitudinal axis. For this reason, dexterity and force feedback at the tip of the surgical tool are strongly reduced. Furthermore, in cases of a larger prostate, there can be some difficulties in manipulating the resectoscope [13]. These issues may affect the outcome of surgery in the procedures (related to Ho:YAG and Tm:YAG laser) that require direct contact between the laser and prostatic tissue. In particular, the closer the contact, the better is the distribution of laser energy; consequently, energy loss by water absorption is minimized, tissue ablation is more homogeneous avoiding formation of craters (that can entrap tissue fragments, debris, and perfusion liquid that partially absorb and scatter the incident light, thus, hindering laser effect [20]).

Laser-assisted surgical procedures can be efficient and cost effective for the BPH treatment with better long-term surgical outcomes compared with the conventional TURP or open prostatectomy. However, a steep operative learning curve caused by the previously discussed issues may be an obstacle to the widespread use of these techniques. Moreover, surgical outcomes are currently variable and dependent on the experience and technical ability of the urologic surgeon [13]. The limitations of the current laser instrumentation play a critical role in the ability of surgeons to deliver consistent care. Advancement in the instrumentation with the aim of providing dexterity and force feedback at the tip of the surgical tool can potentially improve the laser-assisted BPH treatment, and final patient outcomes.

We decided to focus our clinical target on the Ho:YAG laser (that is currently widely applied in BPH procedures). In particular, the surgical procedure we focused on is HoLRP that is a well established procedure, guarantees to collect tissue specimen, and does not strictly require the use of a morcellator; therefore, the ASTRO system needs to be compatible only with the resectoscope instrumentation.

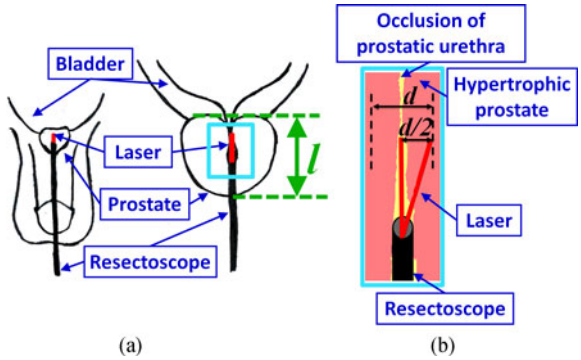

Fig. 2. Laser tip steering: definition of requirements for the actuation unit: (a) overview of the laser procedure for BPH; (b) close view of the laser in the prostatic urethra.

III. Design and Fabrication of the ASTRO Platform

The design and fabrication of the ASTRO robotic platform for transurethral laser-assisted surgery of BPH is described in the present Section. The proposed system is composed of a catheter-like robot, integrated in a commercial resectoscope operative channel, provided with a cable-driven actuation mechanism and an optical fiber-based sensing unit. The design requirements of the robotic platform along with design details and system components are discussed in the following.

A. Design Requirements

During the design phase of the ASTRO system, clinical and technical specifications have been analyzed.

The system must be inserted into the operative channel of a commercial resectoscope working element, which typically has a maximum diameter of 2.5 mm. The resectoscope working element used for this study is the Karl Storz 27042 LV (https://www.karlstorz.com), with an operative channel of 2.5 mm. Furthermore, ASTRO needs to integrate a commercial laser fiber for prostatic tissue ablation; typical diameter of the laser fiber is 0.8–1 mm. The laser fiber used in this study is provided by El.En. SpA (http://www.elengroup.com): it has a diameter of 1 mm and it is a lateral emission fiber, thus it emits the laser light beam at 90° to the fiber direction.

ASTRO has to integrate both an actuation mechanism for enhancing distal dexterity and steering the laser fiber, and a contact sensing system for contact monitoring between laser and tissue.

The actuation mechanism of the ASTRO system has to guarantee a sufficient steering of the laser fiber in order to establish contact between the surgical tool and the prostatic tissue during the treatment. Nevertheless, the steering of the laser fiber has to be restrained in order to avoid risks such as perforations [18]. The diameter of a healthy prostatic urethra is around 6 mm and its length is around 30 mm (shown as d and l in Fig. 2). In BPH, the prostate is enlarged and the prostatic urethra is occluded. Considering these anatomical dimensions, a laser tip

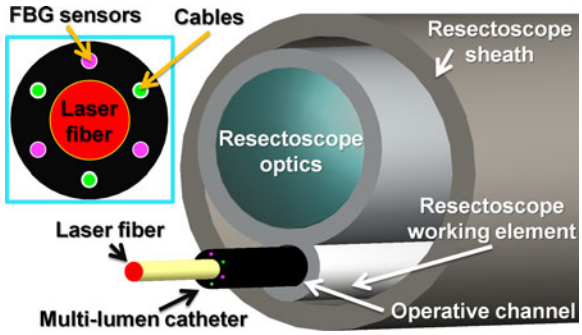

Fig. 3. Schematic overview of the ASTRO system design. In the inset, section of the multilumen catheter integrating the laser fiber, the FBG sensors (in pink) and actuation cables (in green) is shown.

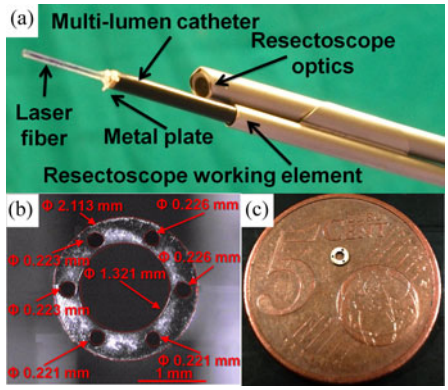

Fig. 4. Multilumen catheter: (a) tip of the ASTRO system, with the multilumen catheter inserted in the resectoscope, (b) picture of the multilumen section at the optical microscope, (c) metal plate to fix the cables on a 5 cent euro coin.

displacement of $\pm$ 3 mm (shown as *d/2* in Fig. 2) is estimated to be appropriate to establish contact and safe to avoid risks of perforations for the specific application (HoLRP is mainly suitable for small prostates, therefore a larger steering range may increase the risk of perforation of the prostate capsule).

In laser-assisted BPH surgery, contact monitoring is of outmost importance for the effectiveness of the procedure (see Section II). The ASTRO sensing system needs to achieve a sub-Newton sensitivity and a scanning frequency greater than 100 Hz, in order to provide a quick and precise contact monitoring. The sensing unit location should be inside the prostate, close to the distal end of the surgical tool, in order to directly measure the contact forces between the laser tip and tissue, without artifacts. The sensors must be easy to install, biocompatible, sterilizable, and safe for the patient; in addition, it is preferable that the sensors have no cabling, thus avoiding risks due to electrical powering at the sensor. Finally, the sensing unit must not interfere with the overall size of the surgical instrument, therefore, the sensors should be small in size.

In the laser surgical treatment of BPH, tissue is removed locally by heating at around 100 °C [19]. In order to guarantee the overall safety of the system, ASTRO components need to be compatible with this ablation temperature. Anyway, the temperature drops dramatically as soon as we move away from the ablation site, because of saline solution's continuous flow through the resectoscope sheath (see Fig. 3).

According to the aforementioned specifications, a flexible catheter-like robot has been selected and designed. A schematic overview of the ASTRO system design is shown in Fig. 3. The system is composed of a multilumen catheter that integrates the laser fiber, an actuation mechanism, and a contact sensing system. The multilumen catheter design is discussed in Section III-B. The ASTRO system is provided with a cable-driven actuation unit. Three cables are distributed at 120° intervals in the section of the catheter, in order to steer the laser in all directions. Details regarding actuation unit design are reported in Section III-C. Fiber Bragg grating (FBG) sensors have been selected for the contact sensing system. FBG are fiber optic sensors whose principle of operation is to monitor the shift in wavelength of the returned "Bragg" signal with the changes in the measurand (i.e., strain and temperature) [21]. In this study, FBG sensors serve to monitor the strain, therefore, they must be glued inside the multilumen catheter, and so the laser fiber. In recent research studies, FBG sensors have been applied in ophthalmology [22], [23], urology [24], colonoscopy [25], needle biopsy [26], and cardiac surgery [27], [28]. FBG sensors hold a great potential for biomedical applications [29] due to their interesting properties such as small size, biocompatibility, sterilizability, chemical inertness, electromagnetically inert nature, high sensitivity, and low cost. In particular, FBG sensors have been employed as contact force sensors for vitreoretinal microsurgery in [22] and [23], prostate needle insertion [24], and cardiac ablation in [27] and [28]. An extensive review of existing approaches on fiber optic contact force sensors for catheterization procedures can be found in [30], and a review on FBG-based contact force sensors for minimally invasive surgical procedures is presented in [31]. The contact sensing unit design of the ASTRO system is discussed in Section III-D. The ASTRO system overview is detailed in Section III-E.

B. Multilumen

The multilumen catheter [shown in Fig. 4(a) and (b)] is designed with an outer diameter of 2.1 mm, in order to be inserted into the operative channel of the Karl Storz 27042 LV resectoscope working element (2.5-mm diameter), and a central lumen of 1.3 mm, so as to integrate the laser fiber (1-mm diameter). The multilumen is also provided with six small lumens (arranged around the periphery forming the vertices of a hexagon) with a diameter of 0.22 mm to integrate cables for actuation (0.17-mm diameter) and FBG sensors (0.18-mm diameter). Cables are fixed at the tip of the multilumen catheter thanks to a metal plate, shown in Fig. 4(c), fabricated by the Kern HSPC 2522 CNC micromilling machine. The metal plate, bonded to the catheter surface, provides with a stiffer interface where to connect the cables, thus avoiding high stress concentration on the multilumen catheter during steering. In this way, the multilumen catheter is more protected from possible damages.

The multilumen can be sterilized by ethylene oxide (EtO) and beta and gamma rays. The material used for the multilumen catheter is Polyamide 12 (PA12). The Young's modulus of PA12 is 1.1 GPa, thus allowing the multilumen to serve both as a

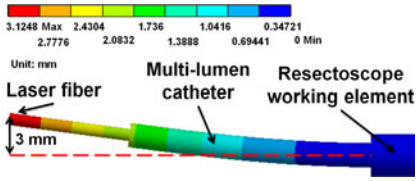

Fig. 5. Finite-element results: computation of total deformation in millimeter of the system when a 12-N pulling force on the cable is applied.

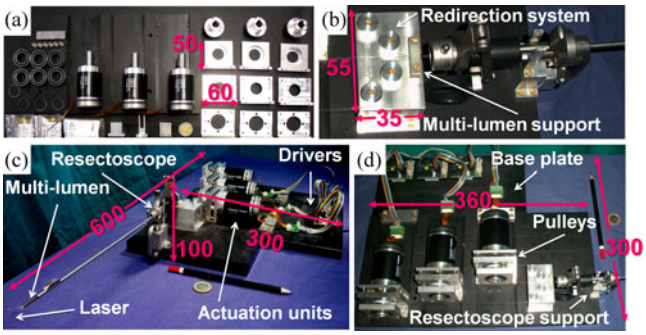

Fig. 6. Actuation unit of the ASTRO system: (a) components of the actuation mechanism, (b) closeup view of multilumen support and redirection system of the cables, (c) assembled actuation system, (d) closeup view of the pulleys.

mechanical continuum for strain transmission between laser and sensors (that have a coating of polyimide with a Young's modulus of 2.5 GPa), but also to be flexible to be bent by actuation cables. The melting point of PA12 (178 °C) is compatible with the laser ablation. The material lubricity (coefficient of friction of 0.28) makes it possible to insert actuation cables and fibers into the lumens, but also to firmly glue the FBG sensors and the laser fiber to the multilumen body.

C. Actuation Mechanism

The necessary pulling force to be applied on a cable in order to reach the required laser displacement (see Section III-A) is estimated with finite-element analysis (FEA), as shown in Fig. 5. The model is implemented in Ansys with the static structural analysis. The model considers the mechanical parameters of the system components: operative channel of the resectoscope working element (stainless steel), multilumen catheter (PA12), cables (HDPE), FBG sensors (core in silica glass and recoating in polyimide), laser fiber (silica glass), etc. The total length of the ASTRO tip is 30 mm (dimensioned considering the length of a healthy prostatic urethra, see Section III-A): the multilumen protrudes out the resectoscope working element 20 mm and the laser protrudes out the multilumen 10 mm. The required pulling force resulted in 12 N.

According to the previously described specifications, three actuation units are integrated in the ASTRO system, as shown in Fig. 6. A double-bending DOF cable mechanism is chosen instead of a single bending plus manual twisting so as to avoid rolling the whole system around its z-axis of $\pm 180°$ from the outside of the patient, to reach all points to be treated within the prostate. In addition, this rolling procedure would produce difficulty in transmitting the rotational motion to the laser tip (due

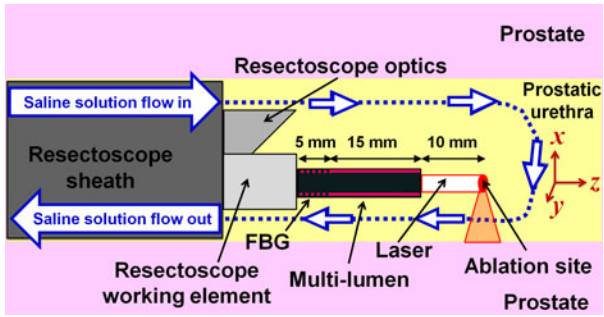

Fig. 7. Schematic representation of the ASTRO sensing system design: FBG positioning within the ASTRO system (FBG sensors are integrated inside the multilumen catheter and two of them are visualized in the picture for clarity).

to friction with the tissues) and would cause stretching of surrounding tissue. In particular, three brushless dc motors (EC-45 Flat-339281, Maxon Motor, Switzerland) with gear head of 19:1 reduction ratio (GP-42C-203117, Maxon Motor, Switzerland) have been selected [see Fig. 6(a)]. Motor control is performed using commercial drivers (EPOS2 24/2 390003 position controllers, Maxon Motor, Switzerland), shown in Fig. 6(c). The three motors are, respectively, connected to three pulleys with a diameter of 3 cm. The actuation units are designed to be fixed on a base plate provided with a dedicated support for the resectoscope and for the multilumen [see Fig. 6(b) and (d)]. The multilumen support is a mechanical stop that allows fixing the multilumen at 20 mm out of the resectoscope distally. Cables are wound on the pulleys, conducted into the multilumen catheter with a redirection system and fixed at the tip of the multilumen catheter at 120° intervals thanks to the metal plate. Nonabrasive Dyneema cables have been chosen with a diameter of 0.17 mm (and a rated load of 215 N), thus allowing insertion and sliding inside the dedicated lumens of the multilumen catheter. The total pulling force of the designed actuation system is 44 N. The actuation unit is designed with a safety factor of 3.6 with respect to the FEA results. The cables are designed with a safety factor of 4.8 with respect to the total pulling force of the designed actuation system.

D. Sensing System

1) Design and Integration: FBG sensors are used for the ASTRO contact monitoring system. These sensors are sensitive to both temperature and strain; the shift in Bragg wavelength $\Delta\lambda$ is expressed as

$$\Delta\lambda = k_\varepsilon \varepsilon + k_T \Delta T \tag{1}$$

where k_ε is the strain sensitivity, ε is the strain, k_T is the temperature sensitivity, and ΔT is the variation of temperature. In order to compensate for temperature effects and measure only the strain, redundant FBG sensors can be used, as for electrical strain gauges. Three FBG sensors are integrated with 120° intervals into the multilumen catheter (refer to Fig. 3). The sensing element (i.e., the Bragg grating) is positioned at about 25-mm distance from the ablation site, i.e., the laser tip, as shown in Fig. 7). The laser tip protrudes out the multilumen 10 mm. Due to this arrangement, sensors experience the same ΔT, but

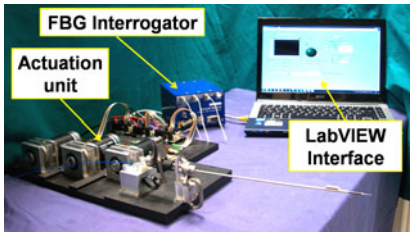

Fig. 8. Schematic representation of the system showing the contact force and pulling force contribution to the local strain at the FBG sensors embedded in the ASTRO system: (a) bending moment M_c caused by the contact force on the prostatic tissue F_c and the bending moment M_p caused by the pulling force exerted on the cables F_p; (b) cross-sectional view showing the contact force F_c and its moment arm L, and the pulling force F_p and its moment arm d. The decoupling of the components is a convention, consequence of the chosen coordinate system (principal axes of the system).

different strain in terms of compression and tension, and therefore, temperature compensation can be performed. As stated in Section III-A, the ablation temperature drops dramatically as soon as we move away from the ablation site, therefore, the laser will not affect the FBG sensors operation.

SmartFBG (Smart Fibres Ltd., U.K.) are integrated in the ASTRO platform. The selected sensors are polyimide fiber with polyimide recoat, which is the recommended combination for strain sensing (http://www.smartfibres.com/); they have a strain sensitivity of 1.2 pm/$\mu\varepsilon$ and a strain range of $\pm$ 9000 $\mu\varepsilon$. Diameter of the fiber is 0.18 mm, grating length is 5 mm, and distance from the grating to the tip of the fiber is 15 mm (see Fig. 7). The centre Bragg wavelength is 1550 nm for all three sensors, thus avoiding possible optical interferences with typical wavelengths of laser fibers for prostate treatment (see Section II). The SmartScan interrogator (Smart Fibres Ltd., U.K.) is used to sample the FBG sensors at a 2.5-kHz refresh rate (resolution of 0.39 pm).

The Epo-Tek 301 optical adhesive is used to glue the FBG sensors and the laser fiber in the multilumen catheter. Since the volume in which to pour the glue is very low, a low-viscosity glue is used to facilitate the casting of the glue. The selected glue has a 100–200 cPs viscosity (at 23 °C, at 100 r/min). Furthermore, the Epo-Tek 301 is nontoxic, it resists to the most common sterilization methods, it has a fast curing time and it has an operating temperature range of up to 300 °C, which is compatible with the laser application. The assembly procedure description is the following: first the optical fibers are inserted in the lumens of the multilumen catheter, then the multilumen is kept in a vertical position in order to facilitate the flow down of the glue, and at this point, the glue is inserted inside the lumens by using a microneedle (0.16-mm diameter) mounted on a syringe. The glue curing time is 24 h at room temperature.

2) Calibration: The aim of the calibration is to correlate the contact force F_c (shown in Fig. 8) applied at the ASTRO tip with the response of the sensors. The components of the force to be monitored are F_{cx} along the x-axis and F_{cy} along the y-axis. The force component along the z-axis F_{cz} is not of interest since the laser fiber is a lateral emission fiber (see Section III-A).

Assuming we can apply the constitutive equations of the beam theory (Navier's equation for stress distribution) to the system and the principle of superposition, the local strain at the FBG sensors embedded in the ASTRO system, is linearly dependent on the bending moment M_c caused by the contact force on the prostatic tissue F_c, and the bending moment M_p caused by the pulling force exerted on the cables F_p (see Fig. 8). The local strain can then be expressed as

$$\varepsilon_{\mathrm{FBG}} = \frac{M_c + M_p}{EI} r = (F_c L + F_p d)\frac{r}{EI} \tag{2}$$

where $\varepsilon_{\mathrm{FBG}}$ is the local strain at the FBG sensor, M is the bending moment, r is the radial distance between the bending neutral axis and the FBG sensor, E is the Young's modulus, I is the moment of inertia, F_c is the contact force, L is the moment arm of the force F_c, F_p is the pulling force, and d is the moment arm of the force F_p (see Fig. 8). Combining (1) and (2) we can write

$$\Delta\lambda_{\mathrm{tot}} = k_\varepsilon (F_c L + F_p d)\frac{r}{EI} + k_T \Delta T. \tag{3}$$

The parameters L, d, r, E, and I are only related to the design of the system, and therefore, are constant. The wavelength shift of the three sensors is, therefore, related to three contributions (contact, pulling, and temperature) and can be expressed as

$$\Delta\lambda_{\mathrm{tot}} = \Delta\lambda_c + \Delta\lambda_p + \Delta\lambda_T \tag{4}$$

where $\Delta\lambda_{\mathrm{tot}}$ is the total wavelength shift, $\Delta\lambda_c$ is the wavelength shift caused by F_c, $\Delta\lambda_p$ is the wavelength shift caused by F_p, and $\Delta\lambda_T$ is the wavelength shift caused by temperature change. We can assume that there is negligible temperature gradient in the small volume in which the sensors are integrated, so the three FBG sensors experience the same ΔT. As demonstrated in [22], by subtracting the mean of the Bragg wavelength shifts of all three FBG sensors, the common mode such as noise, axial strain, and temperature change can be removed. We can then derive the sensor differential signal:

$$\Delta R_i = \Delta\lambda_i - \Delta\lambda_{\mathrm{mean}} = k_{\varepsilon i}\varepsilon_i - \frac{1}{3}\sum_{i=1}^{3} k_{\varepsilon i}\varepsilon_i \tag{5}$$

and (4) can be rewritten as

$$\Delta R_{\mathrm{tot}} = \Delta R_c + \Delta R_p \tag{6}$$

where ΔR_{tot} is the total differential signal and ΔR_c and ΔR_p are, respectively, the differential signals caused by F_c and F_p. At this point, the temperature contribution is compensated, but we still need to discriminate the pulling from the contact. In order to discriminate between the signal caused by the contact forces (ΔR_c) and the signal caused by the pulling forces (ΔR_p) that produce the steering of the laser, thus deriving only the contact forces between the laser fiber and the prostate tissue, calibration experiments are carried out. Since the contributions are coupled, we need to do two separate calibration processes (one applying only contact forces, one applying only pulling forces) to discriminate the components. For the first calibration, known contact transverse forces are applied to the ASTRO tip, without applying tension on the cables (no-steering condition), and wavelength shifts are recorded. Thanks to this calibration, we can relate the contact force with the sensors differential

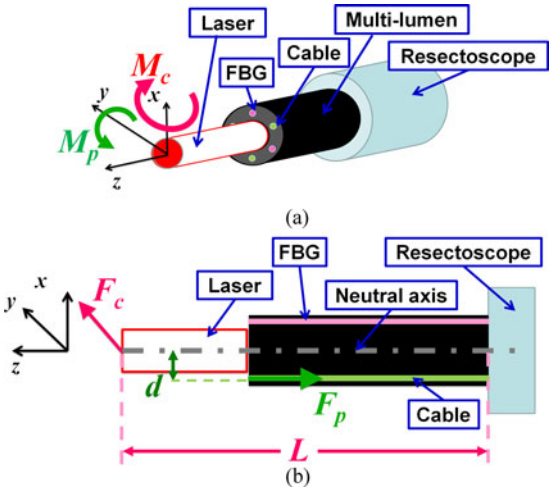

Fig. 9. ASTRO system overview.

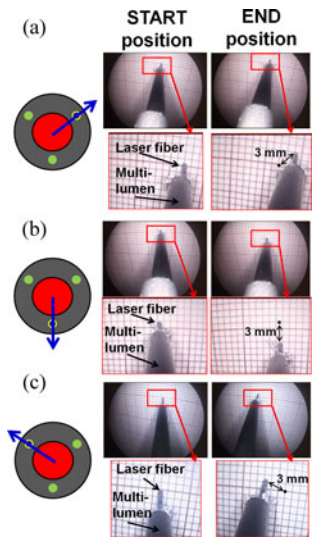

Fig. 10. Actuation assessment. The direction of steering, for each test, is schematically shown in the left part, respectively, in (a), (b), and (c). The laser tip steering, recorded through the resectoscope optics, is shown in the right part of the figures. A close view of the laser tip steering is shown in the bottom of each figure.

signal and obtain:

$$F_c = K\Delta R_c \tag{7}$$

where F_c is a 2×1 vector of the components of the contact force (F_{cx} and F_{cy}) measured by the FBG sensors at the ASTRO tip, K is a 2×3 wavelength-to-force conversion matrix obtained thanks to this calibration step and ΔR_c is a 3×1 vector of the differential signal caused by F_c. As a second step, a calibration phase is carried out in which known laser steering is performed (no-contact-force condition) and wavelength shifts are recorded. Thanks to this calibration, we can derive a coefficient matrix C that relates the sensors differential signal and the laser steering as follows:

$$\Delta R_p = Cd \tag{8}$$

where ΔR_p is a 3×1 vector of the differential signal caused by the laser steering, C is a 3×3 coefficient matrix obtained by this calibration step, and d is a 3×1 vector of the corresponding laser steering values for the three actuation units. At this moment, since the direct kinematics of the system is known (the control of the ASTRO system is based on the standard constant curvature kinematic modeling [32], the derivation of the kinematic model is not reported in this paper), the vector d (position of the end effector) is known. Therefore, using (8), the differential signal ΔR_p can be derived exploiting the matrix C. At this point, we can subtract the contribution ΔR_p of the pulling forces F_p from the total differential signal ΔR_{tot} in (6). Finally, only the contribution ΔR_c of the contact forces F_c is present and contact forces can be derived with (7) using the wavelength-to-force conversion matrix. The calibration phases of the ASTRO system sensing unit are discussed in Section IV-B.

E. Overview of the ASTRO Platform

The overall ASTRO platform is shown in Fig. 9. The platform is composed of a PC running a LabVIEW graphical user interface (GUI) to acquire the signals from the FBG sensors and control actuation motors, the FBG interrogator, and the driving motor platform. The system is currently conceived to provide contact force feedback (via visual and/or auditory signals) to the surgeon by means of the GUI. The ASTRO platform overall dimensions [see Fig. 6(c)] are: 600 mm in length, 300 mm in width, and 100 mm in height. The overall weight is 4 Kg.

IV. Experiments

A. Actuation Assessment

In order to assess the overall ASTRO actuation mechanism performance, the following two tests are carried out.

The ASTRO platform is first positioned so as to point the laser fiber toward a panel of graph paper (see Fig. 10), which serves as a geometric reference during the steering of the laser. Tests are recorded through the optics of the resectoscope. The steering of the laser fiber is successfully performed in all three directions as shown on the left side, respectively, in Fig. 10(a), (b), and (c). The required laser tip displacement of 3 mm, discussed in Section III-A, is achieved in all cases.

A second experimental setup shown in Fig. 11(a) consists of the ASTRO platform inserted in an anthropomorphic phantom that reproduces urethra, prostatic urethra, prostate, and bladder. The anthropomorphic phantom has been developed by the EndoCAS Centre for Computer Assisted Surgery, Cisanello Hospital, Pisa, Italy (http://www.endocas.org/), starting from the study of the physical properties of the tissues involved in the surgical scenario, and from anatomical models derived by 3-D radiological images, in order to mimic tissues mechanical properties and anatomy. Two different laser steering experiments are carried out inside the prostatic urethra phantom: approaching and slicing a tissue. The approaching test, shown in Fig. 11(b) and (c), consists of steering the laser from a central position of the laser fiber inside the urethra to the wall of the prostatic urethra. The slicing test, shown in Fig. 11(d) and (e), consists

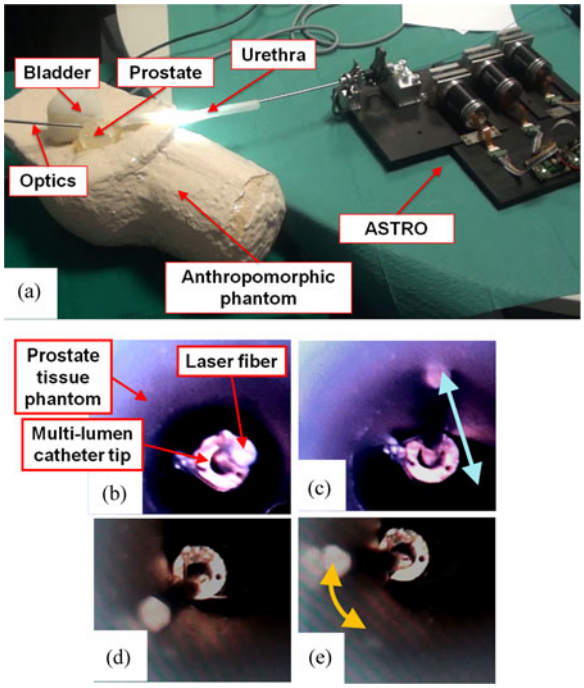

Fig. 11. Actuation assessment test with the anthropomorphic phantom: (a) experimental setup, (b) and (c) approaching phases of the laser tip to the tissue phantom, (d) and (e) slicing phases of the laser tip on the tissue phantom. During experiments, optics is inserted in the phantom so as to point towards the front of the ASTRO system.

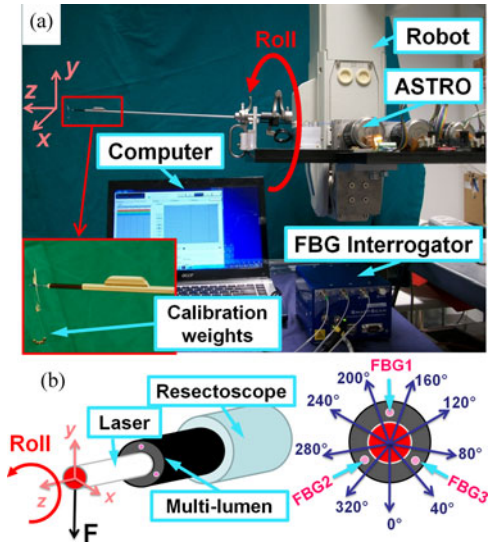

Fig. 12. Calibration setup: (a) picture of the calibration setup showing the ASTRO system mounted on the robot, the FBG interrogator, the computer and calibration weights, (b) schematic representation of the system orientation during calibration (40° rolling angles). Calibration chamber is not shown in the picture.

of steering the laser mimicking the ablation of a portion of the prostatic urethra.

During the actuation assessment tests, the ASTRO platform is controlled by a LabVIEW GUI. The control of the system is based on standard constant curvature kinematic modeling [32], the derivation of the kinematic model is not reported in the paper. These tests show that the laser steering can be performed successfully with the ASTRO actuation mechanism, according to the clinical requirements.

B. Calibration

In order to measure the contact forces exerted at the tip of the ASTRO system (see Section III-D2), two calibration experiments are carried out. The wavelength-to-force conversion matrix K is computed with the first calibration experiment, carried out under no-steering condition. The coefficient matrix C is computed with the second calibration experiment, carried out under no-contact-force condition. The two calibration experiments are described in the following.

1) Calibration Applying Known Contact Forces (No-Steering Condition): In this test, the calibration of the ASTRO platform is carried out applying only known forces on the tip. The calibration setup, shown in Fig. 12, consists of the ASTRO system (with embedded FBG sensors, cables and laser fiber), an industrial 6 degrees-of-freedom (DOF) robot with an angular resolution of 0.05° (RV-3SJB, Mitsubishi Co, Japan), calibration weights, the FBG interrogator, a computer, and a calibration chamber (in order to avoid environmental disturbances, such as temperature variation and air currents). The calibration weights have been weighted before the tests, with an electrically shielded analytical balance, RADWAG Wagi Elektroniczne, which has a readability of 0.1 mg. The ASTRO platform is mounted on the robot, and during calibration, the system orientation is changed by rolling it around the z-axis in a range from 0° to 360° and with step of 40°. In this way, the components of the force, generated by the applied calibration weights, change with respect to the system and the FBG sensors experience different strain (in terms of tension or compression). For each orientation, a load/unload cycle is performed by applying loads: calibration weights are applied at the tip of the system by using a thin wire, with a calibration range from 0 to 2 mN and a calibration step of 0.2 mN. At each step, the corresponding wavelength of the three sensors is recorded. For each orientation, load/unload cycles are repeated ten times. The interrogator is used to sample the three FBG sensors at a 2.5-kHz refresh rate and each acquisition lasts one second. The final log data are 5940 samples (corresponding to the acquisition from the 3 sensors at 9 different orientations, 11 different weights per load/unload cycle, for 10 repetitions) and each sample is the mean value of 2500 (1-s acquisition). Data acquisition and postprocessing are performed, respectively, using the interrogator software SmartSoft (Smart Fibres Ltd., U.K.) and MATLAB (MathWorks, Inc., Natick, MA, USA). The following wavelength-to-force conversion matrix is then obtained by solving (7) using the Moore–Penrose pseudoinverse (least-square solution):

$$K = \begin{pmatrix} -37.4756 & -11.6845 & 0.8172 \\ 4.0836 & -40.8700 & -18.0800 \end{pmatrix}. \quad (9)$$

The force components F_{cx} and F_{cy}, estimated with the wavelength-to-force conversion matrix, versus the actual value of the force using linear fitting and the corresponding residual errors are shown in Fig. 13. The slope of the linear fitting is,

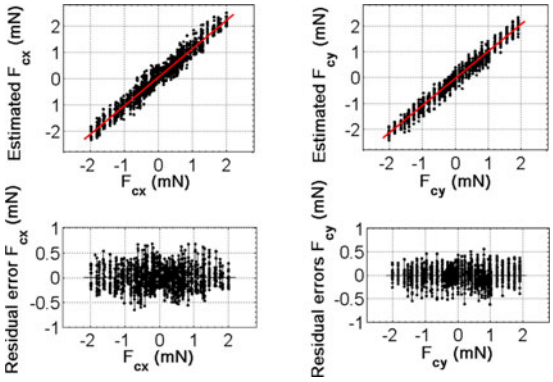

Fig. 13. Calibration results. On the top of the figure, force components F_{cx} and F_{cy}, estimated with the wavelength-to-force conversion matrix, versus the actual value of the force using linear fitting are reported. On the bottom of the figure, corresponding residual errors are shown.

respectively, 1.084 for F_{cx} and 1.052 for F_{cy}. The root mean square error (RMSE) is 0.2083 mN for F_{cx} and 0.1597 mN for F_{cy}.

2) Calibration Performing a Known Steering of the Laser Fiber (No-Contact-Force Condition): In this test, the calibration of the ASTRO platform is carried out applying only tension into cables, thus performing a known steering of the laser fiber. The calibration setup consists of the ASTRO system (with embedded FBG sensors, cables, and laser fiber), the FBG interrogator, a computer, and a calibration chamber. Steering of the laser fiber is performed in all three directions from 0 to 3 mm with a step of 0.5 mm. The system is able to move in intermediate configurations, but during calibration, it is important to test each steering direction separately in order to derive the components of the coefficient matrix C (see Section III-D2). At each step, the corresponding wavelength of the three sensors is recorded. For each direction, load/unload cycles are repeated ten times. The interrogator is used to sample the three FBG sensors at a 2.5-kHz refresh rate and each acquisition lasts one second. The final log data are 1260 samples (corresponding to the acquisition from the three sensors at three different steering directions, seven different steps per load/unload cycle, for ten repetitions) and each sample is the mean value of 2500 (1-s acquisition). The results of this experiment are shown in Fig. 14. The following coefficient matrix composed of the angular coefficient of the curves is obtained:

$$C = \begin{pmatrix} -0.1519 & 0.3404 & -0.1781 \\ 0.3251 & -0.1608 & -0.1783 \\ -0.1561 & -0.1695 & 0.3644 \end{pmatrix}. \qquad (10)$$

Results reported in Fig. 14 show a linear relationship between the steering of the laser fiber and the wavelength shifts of the three FBG sensors, furthermore, a good symmetry is shown. The system hysteresis is computed as the area under the curves for load/unload cycle of pulling forces F_p applied at the ASTRO system versus steering of the laser fiber tip. The pulling force F_p that causes laser steering is computed from the wavelength shifts obtained in this test ΔR_p, with the wavelength-to-force conversion matrix (9). The mean value of the hysteresis is

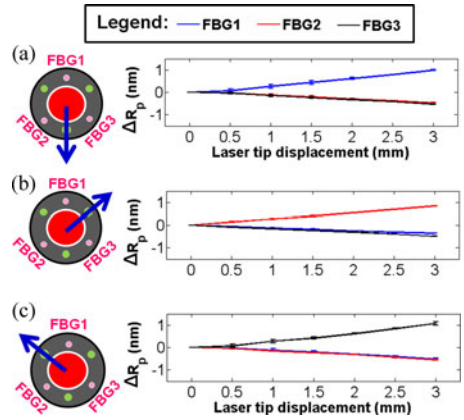

Fig. 14. Calibration results of the ASTRO system under steering (no-contact-force condition). The three sensors differential signals, for the three steering directions are shown. For each graph (a), (b), and (c), the three components of the vector ΔR_p are shown as scalars. The steering directions are shown in the scheme on the left: cables are in green, FBG sensors are in pink.

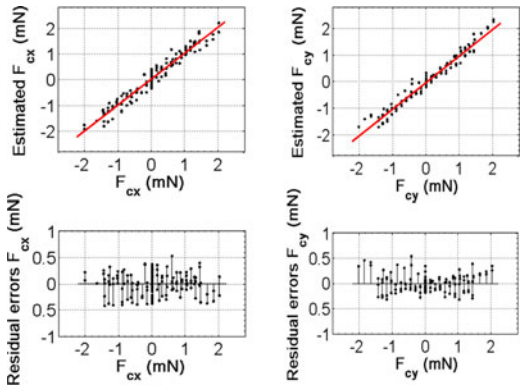

Fig. 15. Validation experiment results. On the top of the figure, force components F_{cx} and F_{cy}, estimated with the wavelength-to-force conversion matrix, versus the actual value of the force using linear fitting are reported. On the bottom of the figure, corresponding residual errors are shown.

0.066×10^{-3} J and 0.073×10^{-3} J, respectively, for the component along the *x*-axis F_{px} and the component along the *y*-axis F_{py}; therefore, it can be considered negligible.

C. Validation

Validation of the ASTRO system sensing unit is described in the following. First, validation is performed testing if the force calculation with the wavelength-to-force conversion matrix (9) can provide reliable force estimation. Second, system validation is carried out, testing if the force calculation can still be performed during laser steering, using the algorithm described in Section III-D2.

1) Validation of the Wavelength-to-Force Conversion Matrix (No-Steering Condition): The purpose of this experiment is to validate at first if the contact force can be estimated correctly without the laser steering. The test is performed applying known forces to the ASTRO tip and no tension on the cables. The experimental setup used is the same as the one discussed in Section IV-B1. The applied forces are in the range from 0 to 2 mN with a step of 0.2 mN and the orientation of the force

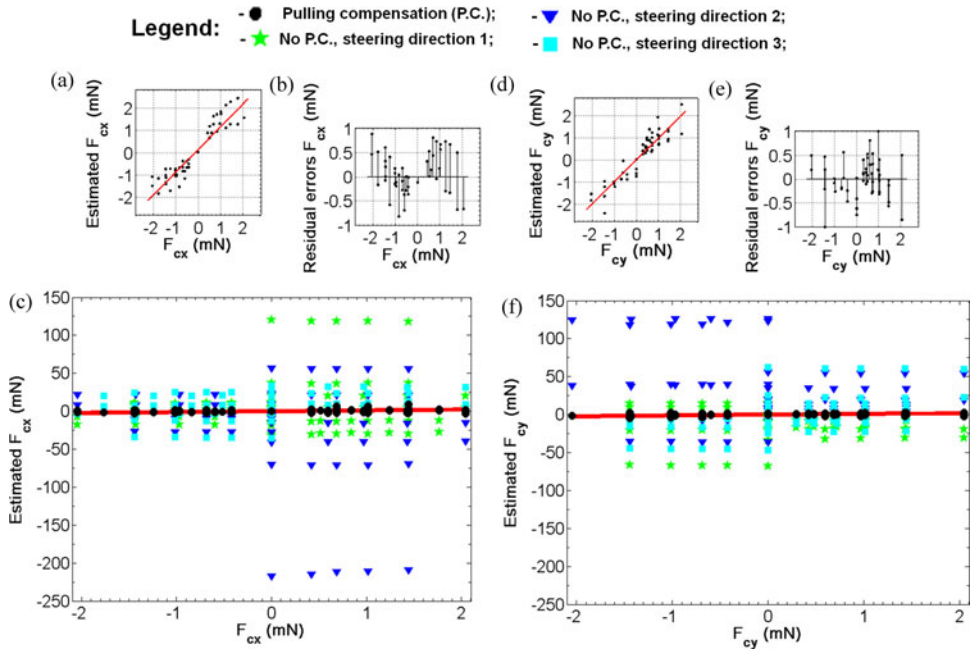

Fig. 16. Validation experiment results: (a) linear fitting of the estimated contact force along the *x*-axis (F_{cx}) with pulling compensation versus the actual value, (b) its residual errors, (c) estimated contact force along the *x*-axis (F_{cx}) with and without pulling compensation versus the actual value, (d) linear fitting of the estimated contact force along the *y*-axis (F_{cy}) with pulling compensation versus the actual value, (e) its residual errors, (f) estimated contact force along the *y*-axis (F_{cy}) with and without pulling compensation versus the actual value.

changes in a range from 0° to 360° and a step of 45°. The force components F_{cx} and F_{cy}, estimated with the wavelength-to-force conversion matrix, versus the actual value of the force using linear fitting and the corresponding residual errors are shown in Fig. 15. The slope of the linear fitting is, respectively, 1 for F_{cx} and 1.002 for F_{cy}. The RMSE is 0.2063 mN for F_{cx} and 0.1701 mN for F_{cy}. The estimation of the force components is consistent with the actual values and with the calibration results.

2) Validation With Steering and Measurement of Contact Forces: The purpose of this experiment is to validate if the contact force can still be estimated correctly during laser steering, using the algorithm described in Section III-D2. The experimental setup used is the same as the one discussed in Section IV-B1. The test is performed applying known forces to the ASTRO tip and performing laser steering. The applied forces range from 0 to 2 mN, with a step of 0.5 mN. The orientation of the force covers the full circle with steps of 45° and 120° (for symmetry). Laser steering is performed in all three directions with a range from 0 to 3 mm and a step of 1.5 mm. The linear fitting of the estimated force component along the *x*-axis F_{cx} versus the actual value of the force, calculated with pulling compensation is shown in Fig. 16(a) and its residual errors are shown in Fig. 16(b). The estimated force component along the *x*-axis F_{cx} versus the actual value of the force without pulling compensation are shown in Fig. 16(c), overlapped to the pulling compensated ones. The linear fitting of the estimated force component along the *y*-axis F_{cy} versus the actual value of the force, calculated with pulling compensation is shown in Fig. 16(d) and its residual errors are shown in Fig. 16(e). The estimated force component along the *y*-axis F_{cy} versus the actual value of the force without pulling compensation are shown in Fig. 16(f), overlapped to the pulling compensated ones. The slope of the linear fitting is, respectively, 1.017 for F_{cx} and 0.9906 for F_{cy}. The RMSE is 0.348 mN for F_{cx} and 0.3389 mN for F_{cy}. This test shows that the estimation of the force during laser steering, with the pulling compensation algorithm, is still consistent with the actual values and with the validation results for the estimation of the force under no-steering condition (see Section IV-C1).

V. Conclusion

The laser-assisted transurethral treatment of BPH is an emerging surgical procedure. Nevertheless, it has still some limitations, e.g., reduced distal dexterity and lacking of force feedback at the surgical tool that influence the outcome of surgery. Automation of the existing technology, with the introduction of robotic tools, could improve the surgical procedure.

In this study, a novel robotic platform for transurethral laser-assisted surgery of BPH is developed. The system combines at the same time distal dexterity and contact monitoring at the surgical site, while maintaining a small distal overall encumbrance and compatibility with current commercial instrumentation (resectoscopes and laser fibers). The ASTRO platform overall dimensions [see Fig. 6(c)] are: 600 mm in length, 300 mm in width, and 100 mm in height. The overall weight is 4 Kg. The platform can possibly be supported by an arm during the surgical procedure so as to compensate for the weight, such as a robotic arm (see Fig. 12) or a Martin's Arm. The surgeon can move the ASTRO system from outside of the patient in an easier way and translate it forward and backwards with respect to its *z*-axis. Designing a smaller actuation stage is part of our future work. The actuation mechanism of the ASTRO platform is tested in

TABLE I
SUMMARY OF THE CALIBRATION AND VALIDATION RESULTS

	RMSE	
	F_{cx}	F_{cy}
Calibration	0.2083	0.1597
Validation (only *Fc* applied)	0.2063	0.1701
Validation (*Fc* and *Fp* applied)	0.348	0.3389

in vitro experiments and proved to be capable of performing laser steering according to the clinical requirements. The sensing system for performing contact monitoring between the laser fiber and the hypertrophic prostatic tissue is characterized with calibration and validation experiments. A contact force calculation method, with the aim of discriminating the contact forces from the pulling forces exerted on the cables, is proposed and validated. The sensing system proved to be capable of monitoring contact, with a sub-Newton sensitivity, in both no laser steering and laser steering condition. If we compare RMSE resulted from calibration and validation tests with only contact force F_c applied (see Table I), we see that the results are consistent: Error affects the second figure. The validation results for the test with both contact force F_c and pulling force F_p applied is still consistent with the calibration results and with validation tests with only contact force F_c applied (see Table I): error affects the first figure, still sub-Newton sensitivity is reached. The dynamic response of the sensing system will be investigated in future experiments.

Ex vivo and *in vivo* tests with clinicians will be performed in future experiments. The authors envisage that these tests will pave the way to study the necessary contact forces during laser-assisted transurethral surgery of the prostate and the necessary dexterity of the laser fiber. This activity will allow to understand which are the best combinations of dexterity and contact forces to be applied in order to improve the ablation procedure. This data, to the best of the authors' knowledge, are not yet known in the literature.

ACKNOWLEDGMENT

The authors would like to thank Mr. M. Pracchia for the support during the fabrication and assembly of the ASTRO platform and the EndoCAS Centre for Computer Assisted Surgery, Cisanello Hospital, Pisa, Italy (http://www.endocas.org/) for making the anthropomorphic phantom available for the tests.

REFERENCES

[1] D. Murphy, B. Challacombe, M. S. Khan, and P. Dasgupta, "Robotic technology in urology," *Postgraduate Med. J.*, vol. 82, no. 973, pp. 743–747, 2006.

[2] S. J. Harris, F. Arambula-Cosio, Q. Mei, R. D. Hibberd, B. L. Davies, J. E. A. Wickham, and B. Kundu, "The probot—An active robot for prostate resection," in *Proc. Inst. Mech. Eng., H, J. Eng. Med.*, vol. 211, no. 4, pp. 317–325, 1997.

[3] R. Goldman, A. Bajo, L. Maclachlan, R. Pickens, S. Herrell, and N. Simaan, "Design and performance evaluation of a minimally invasive telerobotic platform for transurethral surveillance and intervention," *IEEE Trans. Biomed. Eng.*, vol. 60, no. 4, pp. 918–925, Apr. 2013.

[4] W. J. Yoon, S. Park, P. G. Reinhall, and E. J. Seibel, "Development of an automated steering mechanism for bladder urothelium surveillance," *J. Med. Devices*, vol. 3, no. 1, pp. 0110041–0110049, 2009.

[5] M. Aron and M. M. Desai, "Flexible Robotics," *Urol. Clin. North Amer.*, vol. 36, no. 2, pp. 157–162, 2009.

[6] R. Chopra, A. Colquhoun, M. Burtnyk, W.A. N'djin, I. Kobelevskiy, A. Boyes, K. Siddiqui, H. Foster, L. Sugar, M. A. Haider, M. Bronskill, and L. Klotz, "MR imaging-controlled transurethral ultrasound therapy for conformal treatment of prostate tissue: Initial feasibility in humans," *Radiology*, vol. 265, no. 1, pp. 303–13, 2012.

[7] R. Seifabadi, E. E. Gomez, F. Aalamifar, G. Fichtinger, and I. Iordachita, "Real time tracking of a bevel tip needle with varying insertion depth toward teleoperated MRI guided needle steering," in *Proc. IEEE/RSJ Int. Conf. Intell. Robots Syst.*, 2013, pp. 469–479.

[8] W. Shang, H. Su, G. Li, and G. S. Fischer, "Teleoperation system with hybrid pneumatic-piezoelectric actuation for MRI-guided needle insertion with haptic feedback," in *Proc. IEEE/RSJ Int. Conf. Intell. Robots Syst.*, 2013, pp. 4092–4098.

[9] R. Hashimoto, D. Kim, N. Hata, and T. Dohi, "A tubular organ resection manipulator for transurethral resection of the prostate," in *Proc. IEEE/RSJ Int. Conf. Intell. Robots Syst.*, 2004, vol. 4, pp. 3954–3959.

[10] A. J. Pantuck, J. Baniel, Z. Kirkali, T. Klatte, N. Zomorodian, O. Yossepowitch, and A. S. Belldegrun, "A novel resectoscope for transurethral resection of bladder tumors and the prostate," *J. Urol.*, vol. 178, no. 6, pp. 2331–2336, 2007.

[11] G. Ho, W. S. Ng, M. Y. Teo, C. K. Kwoh, and W. S. Cheng, "Computer-assisted transurethral laser resection of the prostate (CALRP): Theoretical and experimental motion plan," *IEEE Trans. Biomed. Eng.*, vol. 48, no. 10, pp. 1125–1133, Oct. 2001.

[12] S. A. Pierre and D. M. Albala, "The future of lasers in urology," *World J. Urol.*, vol. 25, no. 3, pp. 275–283, 2007.

[13] M. Kim, H. E. Lee, and S. J. Oh, "Technical aspects of holmium laser enucleation of the prostate for benign prostatic hyperplasia," *Korean J. Urol.*, vol. 54, no. 9, pp. 570–579, 2013.

[14] S. Gravas, A. Bachmann, O. Reich, C. G. Roehrborn, P. J. Gilling, and D. L. J. Rosette, "Critical review of lasers in benign prostatic hyperplasia (BPH)," *BJU Int.*, vol. 107, no. 7, pp. 1030–1043, 2011.

[15] K. T. McVary, "Clinical evaluation of benign prostatic hyperplasia," *Rev. Urol.*, vol. 5, pp. S3–S11, 2003.

[16] A. Thorpe and D. Neal, "Benign prostatic hyperplasia. *Lancet*, vol. 361, no. 9366, pp. 1359–1367, 2003.

[17] B. Rocco, G. Albo, R. C. Ferreira, M. Spinelli, G. Cozzi, P. Dell'Orto, and F. Rocco, "Recent advances in the surgical treatment of benign prostatic hyperplasia," *Therapeutic Adv. Urol.*, vol. 3, no. 6, pp. 263–272, 2011.

[18] R. M. Kuntz, "Laser treatment of benign prostatic hyperplasia," *World J. Urol.*, vol. 25, no. 3, pp. 241–247, 2007.

[19] N. M. Fried, "New laser treatment approaches for benign prostatic hyperplasia," *Current Urol. Rep.*, vol. 8, pp. 47–52, 2007.

[20] H. W. Kang, J. Kim, and Y. S. Peng, "*In Vitro* investigation of wavelength-dependent tissue ablation: Laser prostatectomy between 532 nm and 2.01 μm," *Lasers Surg. Med.*, vol. 42, no. 3, pp. 237–244, 2010.

[21] A. D. Kersey, M. A. Davis, H. J. Patrick, M. LeBlanc, K. P. Koo, C. G. Askins, and E. J. Friebele, "Fiber Grating Sensors," *J. Lightw. Technol*, vol. 15, no. 8, pp. 1442–1463, Aug. 1997.

[22] X. He, J. Handa, P. Gehlbach, R. Taylor, and I. Iordachita, "A sub-millimetric 3-DOF force sensing instrument with integrated fiber Bragg grating for retinal microsurgery," *IEEE Trans. Biomed. Eng.*, vol. 61, no. 2, pp. 522–534, Feb. 2014.

[23] B. Gonenc, J. Handa, P. Gehlbach, R. H. Taylor, and I. Iordachita, "Design of 3-DOF Force Sensing Micro-Forceps for Robot Assisted Vitreoretinal Surgery," in *35th Annu. Int. Conf. IEEE Eng. Med. Biol. Soc.*, Jul. 2013, pp. 5686–5689.

[24] R. Monfaredi, R. Seifabadi, G. Fichtinger, and I. Iordachita, "Design of a decoupled MRI-compatible force sensor using fiber Bragg grating sensors for robot-assisted prostate interventions," *Proc. SPIE*, vol. 8671, pp. 867118–867118, Mar. 2013.

[25] X. Yi, J. Qian, L. Shen, Y. Zhang, and Z. Zhang, "An Innovative 3D colonoscope shape sensing sensor based on FBG sensor array," in *Proc. IEEE Int. Conf. Inform. Acquisition*, Jul. 2007, pp. 227–232.

[26] Y. L. Park, S. Elayaperumal, B. Daniel, S. C. Ryu, M. Shin, J. Savall, and M. R. Cutkosky, "Real-time estimation of 3-D needle shape and deflection for MRI-guided interventions," *IEEE/ASME Trans. Mechatronics.*, vol. 15, no. 6, pp. 906–915, Dec. 2010.

[27] K. Yokoyama, H. Nakagawa, D. C. Shah, H. Lambert, G. Leo, N. Aeby, and W. M. Jackman, "Novel contact force sensor incorporated in irrigated

radiofrequency ablation catheter predicts lesion size and incidence of steam pop and thrombus," *Circulation, Arrhythmia Electrophysiol.*, vol. 1, no. 5, pp. 354–362, 2008.

[28] S. C. M. Ho, M. Razavi, A. Nazeri, and G. Song, "FBG sensor for contact level monitoring and prediction of perforation in cardiac ablation," *Sensors*, vol. 12, no. 1, pp. 1002–1013, 2012.

[29] V. Mishra, N. Singh, U. Tiwari, and P. Kapur, "Fiber grating sensors in medicine: Current and emerging applications," *Sens. Actuators A, Phys.*, vol. 167, no. 2, pp. 279–290, 2011.

[30] P. Polygerinos, D. Zbyszewski, T. Schaeffter, R. Razavi, L. D. Seneviratne, and K. Althoefer, "MRI-compatible fiber-optic force sensors for catheterization procedures," *IEEE Sensors J.*, vol. 10, no. 10, pp. 1598–1608, Oct. 2010.

[31] A. A. Abushagur, N. Arsad, M. I. Reaz, and A. Bakar, "Advances in biotactile sensors for minimally invasive surgery using the fibre Bragg grating force sensor technique: A survey," *Sensors*, vol. 14, no. 4, pp. 6633–6665, 2014.

[32] R. J. Webster and B. A. Jones, "Design and kinematic modeling of constant curvature continuum robots: A review," *Int. J. Robot. Res.*, vol. 29, no. 13, pp. 1661–1683, 2010.

Authors' photographs and biographies not available at the time of publication.